This is the peer-reviewed, final accepted version for American Mineralogist, published by the Mineralogical Society of America.
The published version is subject to change. Cite as Authors (Year) Title. American Mineralogist, in press.
DOI: https://doi.org/10.2138/am-2022-7983. http://www.minsocam.org/

# Reversion 4:

## Zinconigerite-2*N*1*S* $ZnSn_2Al_{12}O_{22}(OH)_2$ and zinconigerite-6*N*6*S* $Zn_3Sn_2Al_{16}O_{30}(OH)_2$, two new minerals of the nolanite-spinel polysomatic series from the Xianghualing skarn, Hunan Province, China

Can Rao[1*], Xiangping Gu[2], Rucheng Wang[3], Qunke Xia[1], Chuanwan Dong[1], Frédéric Hatert[4], Fabrice Dal Bo[5], Xuege Yu[1], and Wumengyu Wang[1]

[1.] Key Laboratory of Geoscience Big Data and Deep Resource of Zhejiang Province, School of Earth Sciences, Zhejiang University, Hangzhou 310027, China
[2.] State Key Laboratory for Mineral Deposits Research, School of Earth Sciences and Engineering, Nanjing University, Nanjing, 210046, China
[3.] School of Earth Sciences and Info-physics, Central South University, Changsha, 410083, China
[4.] Laboratoire de Minéralogie, B18, Université de Liège, B-4000 Liège, Belgium
[5.] Natural History Museum, University of Oslo, PO 1172 Blindern, 0318 Oslo, Norway
*E-mail: canrao@zju.edu.cn

## ABSTRACT

Zinconigerite-2*N*1*S* $ZnSn_2Al_{12}O_{22}(OH)_2$ and zinconigerite-6*N*6*S* $Zn_3Sn_2Al_{16}O_{30}(OH)_2$ are two new minerals with different numbers and ratios of nolanite (*N*) and spinel (*S*) modules. Both phases have been discovered in the Xianghualing skarn, Hunan Province, China. Zinconigerite-2*N*1*S* (zn-2*N*1*S*) and zinconigerite-6*N*6*S* (zn-6*N*6*S*) are named for their chemical composition, number and ratios of *N*-*S* modules, according to the nomenclature of the nolanite-spinel polysomatic series of Armbruster (2002). Both phases occur as aggregates, sub-to-euhedral crystals, with maximal dimensions up to 100 μm, within fluorite aggregates, and are closely associated with phlogopite, chrysoberyl, magnetite, cassiterite, margarite, and nigerite-taaffeite group minerals. They do not show fluorescence in long- or short-wave ultraviolet light.

The calculated densities are 4.456 g/cm$^3$ for zn-2*N*1*S* and 4.438 g/cm$^3$ for zn-6*N*6*S*. Optically, zn-2*N*1*S* is uniaxial (+) with ω = 1.83 (1), ε = 1.84 (2); zn-6*N*6*S* is uniaxial (+) with ω = 1.85 (1), ε = 1.87 (2) (λ = 589 nm). Their chemical compositions by electron-microprobe analyses give the empirical formulas $(Zn_{0.734}Mn_{0.204}Na_{0.122}Ca_{0.063}Mg_{0.044})_{\sum 1.166}(Sn_{1.941}Zn_{0.053}Ti_{0.007})_{\sum 2}(Al_{11.018}Fe^{3+}_{0.690}Zn_{0.200}Si_{0.092})_{12}O_{22}(OH)_2$ for zn-2*N*1*S* and $(Zn_{1.689}Mn_{0.576}Mg_{0.328}Fe^{3+}_{0.407})_{\sum 3}(Sn_{1.882}Zn_{0.047}Ti_{0.071})_{\sum 2}(Al_{14.675}Fe^{3+}_{1.088}Na_{0.13}Ca_{0.086}Si_{0.017})_{\sum 15.996}O_{30}(OH)_2$ for zn-6*N*6*S*. Both phases have trigonal symmetry; the unit cell parameters of zn-2*N*1*S* ($P\bar{3}m1$) and zn-6*N*6*S* ($R\bar{3}m$), refined from single-crystal X-ray diffraction data, are, $a$ = 5.7191 (2) and 5.7241 (2) Å, $c$ = 13.8380 (6) and 55.5393 (16) Å, $V$ = 391.98 (3) and 1575.96 (12) Å$^3$, and $Z$ = 1 and 3, respectively. The structure of zn-*2N1S* is characterized by the alternating O-$T_1$-O-$T_2$-O-$T_1$ layers stacked along the *c*-axis, showing the connectivity of *N*-*S*-*N*. Whereas the polyhedral stacking sequence of zn-6*N*6*S* is 3 × (O-$T_1$-O-$T_2$-O-$T_2$-O-$T_1$), reflecting a *N*-*S*-*S*-*N*-*N*-*S*-*S*-*N*-*N*-*S*-*S*-*N* connectivity of the polysomatic structure. The structure of zn-2*N*1*S* shows the elements exchange of Al → Sn and Al → Zn, suggesting the substitution mechanism of 2Al → Zn + Sn. The complex substitution of Zn by multiple elements (Al, $Fe^{3+}$, Mn, Mg) in the structure of zn-6*N*6*S*, is coupled with the low occupancy of Al5-octahedra. $Fe^{3+}$ → Al substitution occurs in Al1-tetrahedra of both zn-2*N*1*S* and zn-6*N*6*S*. The new polysomes, zn-2*N*1*S* and zn-6*N*6*S*, likely crystallize under F-rich conditions during the late stages of the Xianghualing skarn formation. The discovery of zn-2*N*1*S* and zn-6*N*6*S* provide new insights into the crystal chemistry of the *N*-*S* polysomatic series and their origin.

**Key words:** zinconigerite-2*N*1*S*, zinconigerite-6*N*6*S*, nolanite module, spinel module, polysomatic series, Xianghualing skarn

52 ## INTRODUCTION

53 Minerals of the nigerite and högbomite groups are included in a polysomatic series that
54 comprises nolanite and spinel structural blocks. The structures of nigerite and högbomite group
55 minerals are constructed by the regular, stacking of (001) slabs of a nolanite module and (111)
56 slabs of a spinel module (Armbruster 2002). The nolanite module consists of a layer of
57 octahedrally coordinated cations (O-layer) and a layer of both tetrahedrally and octahedrally
58 coordinated cations with an OH group ($T_1$-layer), whereas the spinel module consists of an O-
59 layer and a layer of both tetrahedrally and octahedrally coordinated cations ($T_2$-layer) (Fig. 1).
60 If Sn > Ti in the nolanite module, these minerals belong to the nigerite group; however, if Ti >
61 Sn in the nolanite module, they belong to the högbomite group. Different chemical
62 compositions, number and ratios of nolanite and spinel blocks differentiate members of the
63 nigerite and högbomite groups, such as magnesionigerite-2*N*1*S* (Chen et al. 1989),
64 magnesionigerite-6*N*6*S* (Yang et al. 2013), ferronigerite-2*N*1*S* (Bannister et al. 1947; Jacobson
65 and Webb 1947), ferronigerite-6*N*6*S* (Peacor 1967, Burke et al. 1977), magnesiohögbomite-
66 2*N*2*S* (McKie 1963), magnesiohögbomite-2*N*3*S* (Hejny and Armbruster 2002),
67 magnesiohögbomite-6*N*6*S* (Schmetzer and Berger 1990), zincohögbomite-2*N*2*S* (Ockenga
68 1998), and zincohögbomite-2*N*6*S* (Armbruster et al. 1998). The polysomes of zn-2*N*1*S* and zn-
69 6*N*6*S* have been predicted as members of nigerite group by Armbruster (2002), these phases
70 have not yet been observed.

71 The recent discovery of two new *N*-*S* type minerals from the Xianghualing skarn (Linwu
72 County, Hunan Province, southern China), zn-2*N*1*S* and zn-6*N*6*S*, led to the definition of two
73 new species, which were approved by the Commission on New Minerals, Nomenclature and

Classification, IMA (2018-037 and 2018-122a, respectively) (Rao et al. 2018, 2020). The holotype material has been deposited in the collections of the Geological Museum of China, No. 15 Building, Yangrou Hutong road, Xisi, Beijing 100031, People's Republic of China, under catalog number M13810 (zn-2*N*1*S*) and M13811 (zn-6*N*6*S*). The chemical composition and crystal structure were determined using electron probe microanalysis (EPMA) and single crystal X-ray diffraction (SC-XRD), respectively. This paper describes the chemical and structural information of zn-2*N*1*S* and zn-6*N*6*S*, and discusses the composition, crystal chemistry and crystal structure of *N*-*S* polysomatic series and their petrological origin.

## GEOLOGICAL SETTING, OCCURRENCE, AND PARAGENESIS

The Xianghualing skarn is a tin-polymetallic (Sn-W-Be-Li) deposit in Linwu County, Hunan Province, in southern China. It occurs in the exocontact zone between the Laiziling granitic pluton and the Middle-Upper Devonian carbonate rocks of the Qiziqiao Formation (Huang et al. 1988). The U-Pb dating of the zircon of the protolithionite granite from the Laiziling granitic pluton indicates the age of 155 Ma (Zhu et al. 2011). The Laiziling granite is enriched in the elements Li, Be, Sn, W, Rb, Nb, and Ta; it is generally regarded as the main Sn source of the Xianghualing orebodies (Huang et al. 1988). The granite has an average Sn concentration of 65 ppm (Zhong 2014). The predominant accessory minerals in the Xianghualing skarn include Sn minerals (cassiterite, hulsite, and nigerite group minerals), W minerals (wolframite and scheelite), Be minerals (hsianghualite, liberite, chrysoberyl, hambergite, bertrandite, and taaffeite group minerals), and Li minerals (hsianghualite and liberite). The Xianghualing skarn is the type locality for five minerals species: hsianghualite $Ca_3Li_2Be_3(SiO_4)_3F_2$ (Huang et al. 1958), liberite $Li_2Be(SiO_4)$ (Chao 1964), ferrotaaffeite-2*N*'2*S* $BeFe_3Al_8O_{16}$ (Yang et al. 2012),

97 mengxianminite $Ca_2Sn_2Mg_3Al_8[(BO_3)(BeO_4)O_6]_2$ (Rao et al. 2017), and chukochenite $LiAl_5O_8$
98 (Rao et al. 2020).

99 Both zn-2*N*1*S* and zn-6*N*6*S* occur as aggregates, sub-to-euhedral crystals, with maximal
100 dimensions up to 100 μm, and are found within fluorite aggregates (Fig. 2). The crystals have
101 a stout prismatic morphology, elongated along [001]. The phase of zn-2*N*1*S* is closely
102 associated with fluorite, phlogopite, chrysoberyl, ferronigerite-2*N*1*S*, magnetite, cassiterite,
103 magnesiotaaffeite-2*N*'2*S,* and margarite (Fig. 2a and 2b). The mineral of zn-6*N*6*S* occurs as
104 crystals in interstices of fluorite (Fig. 2c and 2d), or with ferronigerite-2*N*1*S* in veinlets or
105 aggregates in fluorite, in close association with phlogopite, chrysoberyl, ferronigerite-6*N*6*S*,
106 and ferronigerite-2*N*1*S*. Intimate intergrowths with hydrothermal minerals such as fluorite and
107 phlogopite indicate that zn-2*N*1*S* and -6*N*6*S* are of hydrothermal origin in the Xianghualing
108 skarn.
109
110 ## CRYSTAL CHEMISTRY
111 ### Chemical composition
112 The chemical compositions of zn-2*N*1*S*, zn-6*N*6*S*, and coexisting minerals were obtained on
113 polished samples. The analyses were performed using a SHIMADZU EPMA 1720H electron
114 microprobe at the EPMA Lab in the School of Earth Sciences, Zhejiang University, operating
115 in wavelength-dispersive mode at 15 kV, 20 nA beam current, 1 μm beam diameter, and 20 s
116 and 10 s counting times on peak and background regions, respectively. The analytical standards
117 used were orthoclase (Na $K_\alpha$), $MnTiO_3$ (Ti $K_\alpha$), almandine (Ca $K_\alpha$ and Fe $K_\alpha$), obsidian (K $K_\alpha$),
118 pyrope (Mg $K_\alpha$), willemite (Mn $K_\alpha$, Zn $K_\alpha$ and Si $K_\alpha$), topaz (Al $K_\alpha$), cassiterite (Sn $K_\alpha$), and
119 apatite (F $K_\alpha$). F was not detected in either zn-2*N*1*S* or zn-6*N*6*S*. According to the crystal-

stoichiometrical features of zn-2*N*1*S* and zn-6*N*6*S* (see below), Fe is required to be $Fe^{3+}$, thus FeO contents were stoichiometrically converted to $Fe_2O_3$. The contents of $H_2O$ were calculated based on 2 (OH) groups per formula unit (*pfu*). The chemical analysis results of zn-2*N*1*S* and zn-6*N*6*S* are summarized in Table 1.

The empirical formula for zn-2*N*1*S* (based on 24 O *apfu*) is $(Zn_{0.734}Mn_{0.204}Na_{0.122}Ca_{0.063}Mg_{0.044})_{\sum 1.166}(Sn_{1.941}Zn_{0.053}Ti_{0.007})_{\sum 2}(Al_{11.018}Fe^{3+}_{0.690}Zn_{0.200}Si_{0.092})_{\sum 12}O_{22}(OH)_2$. The ideal end-member formula is $ZnSn_2Al_{12}O_{22}(OH)_2$, which requires $Al_2O_3$ 60.30 wt.%, $SnO_2$ 29.71 wt.%, ZnO 8.02 wt.%, and $H_2O$ 1.97 wt.%, total 100.00 wt.%. The empirical formula calculated from the chemical analyses of zn-6*N*6*S* (based on 32 O *apfu*) is $(Zn_{1.689}Mn_{0.576}Mg_{0.328}Fe^{3+}_{0.407})_{\sum 3}(Sn_{1.882}Zn_{0.047}Ti_{0.071})_{\sum 2}(Al_{14.675}Fe^{3+}_{1.088}Na_{0.13}Ca_{0.086}Si_{0.017})_{\sum 15.996}O_{30}(OH)_2$. The ideal end-member formula is $Zn_3Sn_2Al_{16}O_{30}(OH)_2$, which requires $Al_2O_3$ 59.05 wt.%, $SnO_2$ 21.82 wt.%, ZnO 17.68 wt. %, and $H_2O$ 1.45 wt.%, for total 100 wt.%.

**Physical and optical properties**

The crystals of both zn-2*N*1*S* and zn-6*N*6*S* are green and translucent-to-transparent, with vitreous luster. The tenacities are brittle and the fractures are irregular. Neither crystal shows fluorescence in long- or short-wave ultraviolet light. Based on the empirical formula and single-crystal unit-cell parameters, the calculated densities are 4.456 g/cm$^3$ for zn-2*N*1*S* and 4.438 g/cm$^3$ for zn-6*N*6*S*. Optically, zn-2*N*1*S* is uniaxial positive, with $\omega$ = 1.83 (1), $\varepsilon$ = 1.84 (2); zn-6*N*6*S* is also uniaxial positive, with $\omega$ = 1.85 (1), $\varepsilon$ = 1.87 (2) under sodium light ($\lambda$ = 589 nm). The optical orientation is $\alpha$ // *a*, $\beta$ // *b* and $\gamma$ // *c*. According to the calculated density and the measured indexes of refraction, the compatibility indices [1 – ($K_P/K_C$)] of zn-2*N*1*S* and zn-6*N*6*S* are 0.024 and 0.028, respectively, corresponding to the "excellent" category (Mandarino 1981).

This is the peer-reviewed, final accepted version for American Mineralogist, published by the Mineralogical Society of America.
The published version is subject to change. Cite as Authors (Year) Title. American Mineralogist, in press.
DOI: https://doi.org/10.2138/am-2022-7983. http://www.minsocam.org/

## Raman spectroscopy

The Raman spectra of zn-2*N*1*S* and zn-6*N*6*S* were collected using a LabRAM HR evolution Laser Raman microprobe at the School of Earth Sciences at Zhejiang University. A 532 nm laser with a power of 50 mW at the sample surface was used. Silicon (520 $cm^{-1}$ Raman shift) was used as a standard. The Raman spectra were acquired from 100 to 4000 $cm^{-1}$, and the accumulation time of each spectrum was 60 s. The Raman spectra were collected on polished thin sections of zn-2*N*1*S* and zn-6*N*6*S* and are presented in Figure 3. The presence of (OH) groups is confirmed by the Raman shifts at 3476, 3617 and 3699 $cm^{-1}$ for zn-2*N*1*S* (Fig. 3a) and at 3478 $cm^{-1}$ for zn-6*N*6*S* (Fig. 3b). The bands in the region 700–850 $cm^{-1}$ are assigned to the stretching modes $v_1$ and $v_3$ of ($AlO_6$) groups, and the bending modes $v_2$ and $v_4$ of ($AlO_6$) groups in the region of 500–300 $cm^{-1}$. The Zn-O vibration modes are probably at the bands of 634–614 $cm^{-1}$. The lattice vibration modes occur below 310 $cm^{-1}$.

## X-ray crystallography and structure determination

Both powder and single-crystal X-ray diffraction studies were carried out on zn-2*N*1*S* and zn-6*N*6*S*. The powder X-ray diffraction patterns was collected using a Rigaku D/max Rapid IIR micro-diffractometer (Cu *K*a, $\lambda$ = 1.54056 Å) for zn-2*N*1*S* and a Rigaku D/MAX Rapid II micro-diffractometer (Mo *K*α, $\lambda$ = 0.71073 Å) for the zn-6*N*6*S*. The single-crystal X-ray diffraction data for both zn-2*N*1*S* and zn-6*N*6*S* were collected on a Rigaku Synergy diffractometer (Mo *K*α, 50 kV, 1 mA) at the School of Earth Sciences and Info-physics, Central South University (China). The Rigaku CrystalClear software package was used to process structural data, as well as applying Lorentz and polarization corrections. An empirical

absorption correction was applied using the ABSCOR (Higashi 2001) software multi-scan method. Scattering curves for neutral atoms, together with anomalous dispersion corrections, were taken from the *International Tables for X-ray Crystallography* (Volume C) (Wilson 1992).

***Zinconigerite-2N1S***

Single-crystal X-ray diffraction was obtained on a zn-2*N*1*S* crystal fragment measuring 0.120 × 0.075 × 0.050 mm. A total of 3010 reflections were extracted from 624 frames, corresponding to 570 unique reflections. The unit cell parameters, calculated by least squares refinement from these reflections, are $a$ = 5.7191 (2) Å, $c$ = 13.8380 (6) Å, $V$ = 391.98 (3) Å$^3$, and $Z$ = 1. The structure shows trigonal symmetry, and was refined in the space group $P\bar{3}m1$. During the final refinement cycles, all the atoms were refined anisotropically. $R1$ [$F_o > 2s(F_o)$] value of 0.0296 and w$R2$ value of 0.0967 were obtained. Site-occupancies were established by comparing chemical data, site scattering factors, and average bond distances (Table 2a). Selected bond distances and bond valence sums are given in Table 3a and Table 4a, respectively. The powder X-ray diffraction pattern is an excellent match to that of ferronigerite-2*N*1*S* (Arakcheeva et al. 1995), and the ten strongest lines [$d$ in Å($I$)($hkl$)] are 2.841(74)(104), 2.431(100)(113), 1.851(25)(211), 1.834(34)(107), 1.646(74)(214), 1.545(81)(215), 1.428(32)(220), 1.417(27)(305), 1.365(28) (223), and 1.050(39)(325), which gives the unit-cell parameters of $a$ = 5.714 (1) Å, $c$ = 13.821 (3) Å, and $V$ = 390.74 (1) Å$^3$.

The structure of zn-2*N*1*S* is based on a closed-packed oxygen framework, with *N* and *S* modules stacked along the *c*-axis (Fig. 4). The *N* module is composed of one O-layer and one $T_1$-layer. The O-layer is made up of the edge-sharing Al4-octahedra (<Al-O> = 1.956 Å); the $T_1$-layer consists of one Sn-octahedron (<Sn-O> = 2.056 Å), one Al1-tetrahedron (<Al-O> =

187 1.837 Å). The Al1-tetrahedra site is occupied by 0.62 *apfu* Al + 0.38 *apfu* $Fe^{3+}$, and only 0.72
188 *apfu* Al in the Al4-octahedral site; the H atoms are connected to O6 atoms from the O-layer,
189 forming an (OH) group. The *S* module has the approximate formula of gahnite $ZnAl_2O_4$,
190 consisting of one O-layer and one $T_2$-layer; the O-layer is made up of the edge-sharing Al3-
191 octahedra (<Al-O> = 1.920 Å); the $T_2$-layer occurs between two O-layers, is composed of one
192 Al2-octahedra (<Al-O> = 1.899 Å) and two Zn-tetrahedra (<Zn-O> = 1.936 Å) per layer in the
193 unit cell. The site population refinement shows that the tetrahedral site is occupied by 0.49 *apfu*
194 Zn, 0.34 *apfu* Al, 0.10 *apfu* Mn, and 0.07 *apfu* Sn (Table 2a). As shown in Figure 1, in the $T_1$-
195 layers, Sn-octahedra and Al-tetrahedra are corner-sharing, forming zigzag chains along the *a*-
196 and *b*-axes; six-member rings occur between two adjacent zigzag chains, the (OH) is also
197 located in the center of six-member rings. In the $T_2$-layers, each Al-octahedron shares corners
198 with six Zn-tetrahedra, and one Zn-tetrahedron is located in the center of each six-member ring
199 of the Al-octahedra and Zn-tetrahedra. The layer sequence in zn-2*N*1*S* can be described as O-
200 $T_1$-O-$T_2$-O-$T_1$ (*N*-*S*-*N*); therefore, the framework of zn-2*N*1*S* is composed of two *N* (Sn > Ti)
201 modules and one *S* (gahnite) module (Fig. 4).

202 ***Zinconigerite-6N6S***

203 Single-crystal X-ray diffraction data were obtained on a zn-6*N*6*S* crystal fragment
204 measuring 0.020 × 0.045 × 0.030 mm. The crystal structure of zn-6*N*6*S* (Fig. 5) was refined
205 from total 17379 reflections with 857 unique reflections, extracted from 3260 frames, in the
206 range 4.4° < 2θ < 67.4°. The structure shows trigonal symmetry, $a$ = 5.7241(2) Å, $c$ =
207 55.5393(16) Å, $V$ = 1575.96(12) Å$^3$, Z = 3, and was refined in the space group $R\bar{3}m$. In the final
208 refinement cycles, all the atoms were refined anisotropically. $R1$ [$F_o > 2s(F_o)$] and w$R2$ values

are 0.0224 and 0.0574, respectively. Selected bond distances are given in Table 3b, as well as the bond valence sums in Table 4b. The powder X-ray diffraction data indicates that the seven strongest lines [*d* in Å(*I*)(*hkl*)] are 2.846(34)(1 0 16), 2.436(100) (024), 2.424(39)(0 1 20), 1.553(62)(0 3 12), 1.430(61)(220), 0.955(27)(4 1 27), and 0.935(41)(241), which is well matched to that of nigerite-12R (PDF No. 38-0436). The unit-cell parameters refined from the powder data are $a$ = 5.7090(8) Å, $c$ = 55.5342(4) Å, and $V$ = 1567.56(2) Å$^3$.

The structure of zn-6*N*6*S* is composed of six *N* modules and six *S* modules stacked along the *c*-axis (Fig. 5). The *N* module consists of one O-layer of edge-sharing Al5-octahedra (<Al-O> = 1.958 Å) and one $T_1$-layer of Sn-octahedra (<Sn-O> = 2.054 Å) and Al1-tetrahedra (<Al-O> = 1.842 Å). The H atoms in the $T_1$-layer are connected to O atoms in the O1 site of the O-layer, forming an (OH) group. The site population refinement shows that the Al5 octahedral site is only occupied by 0.72 *apfu* Al, the Sn octahedral site by 0.92 *apfu* Sn + 0.08 *apfu* Ti, and the Al1 tetrahedral site by 0.67 *apfu* Al + 0.33 *apfu* $Fe^{3+}$. The *S* module consists of one O-layer of edge-sharing Al2-octahedra (<Al-O> = 1.916 Å) and Al4-octahedra (<Al-O> = 1.920 Å), one $T_2$-layer formed by Al3-octahedra (<Al-O> = 1.908 Å) and Zn-tetrahedra (<Zn-O> = 1.944 Å). The Zn1 and Zn2 sites are occupied by 0.50 *apfu* Zn + 0.23 *apfu* $Fe^{3+}$ + 0.14 *apfu* Mn + 0.08 *apfu* Mg + 0.05 *apfu* Al and 0.37 *apfu* Zn + 0.21 *apfu* Al + 0.20 *apfu* $Fe^{3+}$ + 0.14 *apfu* Mn + 0.08 *apfu* Mg, respectively. As shown in Figure 1, in the O-layers, edge-sharing Al-octahedra form chains running along the *a*-and *b*-axes. In the $T_1$-layers, Sn-octahedra and Al-tetrahedra are adjacent to each other, forming zigzag chains along the *a*- and *b*-axes, (OH) group is also located in the center of the six-member rings of the Sn-octahedra and Al-tetrahedra. The Al- octahedra and Zn-tetrahedra in the $T_2$-layers are adjacent to each other, forming zigzag

This is the peer-reviewed, final accepted version for American Mineralogist, published by the Mineralogical Society of America.
The published version is subject to change. Cite as Authors (Year) Title. American Mineralogist, in press.
DOI: https://doi.org/10.2138/am-2022-7983. http://www.minsocam.org/

chains along the *a*- and *b*-axes. The layer sequence in zn-6*N*6*S* can be described as 3 × (O-$T_1$-O-$T_2$-O-$T_2$-O-$T_1$) (Fig. 5b), suggestive of a $N + S + S + N + N + S + S + N + N + S + S + N$ connectivity of polysomatic structure (Fig. 5a).

# DISCUSSION

## Crystal chemistry and substitution mechanisms

Nigerite group minerals are the members of nolanite-spinel polysomatic series, and several minerals of nigerite group have been reported (*e.g.*, Bannister et al. 1947; Jacobson and Webb 1947; Chen et al. 1989; Yang et al. 2013). The descriptions of these phases have demonstrated that the chemical composition, number, and ratio of both nolanite and spinel modules are responsible for the polysome determination among the nolanite-spinel polysomatic series. The Zn content (0.992 *apfu* for zn-2*N*1*S* and 1.736 *apfu* for zn-6*N*6*S*, Table 1) and structural data (Table 2) indicate the occurrence of a gahnite-type module in nolanite-spinel polysomatic series. The minerals of zn-2*N*1*S* and zn-6*N*6*S* are thus the first known polysomes with gahnite modules in nigerite group minerals. The structure of zn-2*N*1*S* shows the periodic stacking sequence of O-$T_1$-O-$T_2$-O-$T_1$ along the *c*-axis, reflecting the connectivity of two *N* and one *S* modules; while the layer sequence of zn-6*N*6*S* is 3 × (O-$T_1$-O-$T_2$-O-$T_2$-O-$T_1$), exhibiting a connectivity of 6*N* + 6*S* polysomatic model.

Normally, nigerite group minerals and related minerals show trigonal ($P\bar{3}m1$ and $R\bar{3}m$) and/or hexagonal ($P6_3mc$) symmetries; the structures with an odd sum of *N* and *S* modules commonly have the symmetry of $P\bar{3}m1$, those with an even sum of both *N* and *S* modules show $P6_3mc$ symmetry (Verma and Krishna 1966). However, zn-6*N*6*S,* with even sum of *N* and *S* modules, is trigonal with the space group of $R\bar{3}m$ (Fig. 5). This may be attributed to its O-layers

253 sandwiched between two $T_1$-layers, and with hydroxyl on both sides (Hejny and Armbruster
254 2002).

255 In the *N* modules of both zn-2*N*1*S* and zn-6*N*6*S*, the Al occupancy of O layers between two
256 $T_1$-layers is less than 1. The Al4 site is only occupied by 0.72 *apfu* Al in zn-2*N*1*S*, and the Al5
257 site is also occupied by 0.72 *apfu* Al in zn-6*N*6*S*. And (OH) groups in both zn-2*N*1*S* and zn-
258 6*N*6*S* (Fig. 4 and Fig. 5), connect with oxygen in the O-layers. The low bond-valence sum of
259 1.47 v.u. observed at O6 is in agreement with it being an (OH) group, and the low bond-valence
260 sum of 1.49 v.u. at O1 in zn-6*N*6*S*. The Raman shifts at 3478 $cm^{-1}$ (Fig. 3) also demonstrate
261 the presence of (OH) in both zn-2*N*1*S* and zn-6*N*6*S*. In addition, all Fe occupies the tetrahedral
262 sites in both zn-2*N*1*S* and zn-6*N*6*S*, and $Fe^{3+}$ (0.49 Å) has relatively smaller radius than $Fe^{2+}$
263 (0.63 Å) (Shannon, 1976), suggesting the calculation of Fe into $Fe^{3+}$ (Table 1 and Table 2).

264 In the crystal structure of zn-2*N*1*S*, the tetrahedral sites of $T_2$-layers are predominantly
265 occupied by 0.49 *apfu* Zn, but also contain 0.34 *apfu* Al, 0.10 *apfu* Mn, and 0.07 *apfu* Sn, and
266 the octahedral sites in $T_1$-layer are occupied by 0.90 *apfu* Sn + 0.10 *apfu* Al (Table 2a). These
267 features reflect the substitution of Al → Sn in Sn-octahedra, and (Al,Mn,Sn) → Zn in the
268 tetrahedral sites of $T_2$-layers, suggesting the substitution mechanism of 2Al → Zn + Sn in the
269 crystal structure of zn-2*N*1*S*. The substitution of Al or Sn → Zn may agree with the low
270 occupancy of the Al4 site. The tetrahedral sites of $T_1$-layers are occupied by 0.62 Al + 0.38
271 $Fe^{3+}$, reflecting the substitution of $Fe^{3+}$ → Al in Al-tetrahedra.

272 Similarly, in the crystal structure of zn-6*N*6*S* (Fig.5 and Table 2b), the octahedral sites in
273 $T_1$-layers are occupied by 0.92 *apfu* Sn + 0.08 *apfu* Ti, suggesting the substitution of Ti → Sn.
274 The Zn1 and Zn2 tetrahedral sites in $T_2$-layers, are occupied by 0.50 *apfu* Zn + 0.23 *apfu* $Fe^{3+}$

This is the peer-reviewed, final accepted version for American Mineralogist, published by the Mineralogical Society of America.
The published version is subject to change. Cite as Authors (Year) Title. American Mineralogist, in press.
DOI: https://doi.org/10.2138/am-2022-7983. http://www.minsocam.org/

275 + 0.14 *apfu* Mn + 0.08 *apfu* Mg + 0.05 *apfu* Al and 0.37 *apfu* Zn + 0.21 *apfu* Al + 0.20 *apfu*
276 $Fe^{3+}$ + 0.14 *apfu* Mn + 0.08 *apfu* Mg, respectively. These features suggest the complex
277 substitution of Zn by multiple compositions of Al, $Fe^{3+}$, Mn, Mg, it may be coupled with the
278 low occupancy of Al5-octahedra. The tetrahedral Al1 sites from $T_1$-layers are occupied by 0.67
279 *apfu* Al + 0.33 *apfu* $Fe^{3+}$, also suggesting the substitution of $Fe^{3+} \rightarrow$ Al.

280 Lithium has been reported to be present in nigerite group minerals. For example, the zn-
281 6*N*6*S* from the Tsomtsaub tin mine (Namibia) contains up to 0.70 wt.% $Li_2O$ (Armbruster and
282 Feenstra 2004), and the magnesionigerite-6*N*6*S* from the Xianghualing skarn has up to 0.74
283 wt.% $Li_2O$, which substitutes $Al^{3+}$ in the octahedral sites of O-layers between two $T_1$-layers,
284 suggesting the substitution of Li + 2(Sn, Ti) → 3Al (Yang et al. 2013). Because it is impossible
285 to analyze Li by using EMPA, the occurrence of Li in the crystals investigated here could not
286 be established. But Li may substitute Al, the low occupancy in the Al4 octahedral site (0.72 Al,
287 zn-2*N*1*S*) and in the Al5 octahedral site (0.72 Al, zn-6*N*6*S*) may indicate the presence of a very
288 little amount of Li in both zn-2*N*1*S* and zn-6*N*6*S*.

289 **Cell parameters and relations to other *N*-*S* polysomatic series minerals**

290 Several polytypes of nigerite-högbomite minerals, 2*N*1*S*, 2*N*2*S*, 2*N*3*S*, 2*N*4*S*, 2*N*5*S*, 2*N*6*S*,
291 6*N*3*S*, 6*N*6*S*, 6*N*9*S* and 6*N*12*S,* have been reported and predicted in nolanite-spinel polysomatic
292 series (*e.g.*, Hejny and Armbruster 2002; Armbruster 2002). However, Be occupying the
293 tetrahedral site in nolanite modules results in a *N'* slab, with composition $BeTM_4O_8$, where T
294 and M represent tetrahedrally and octahedrally coordinated cations; this corresponds to
295 taaffeite-group minerals (Armbruster 2002). Nigerite-, högbomite- and taaffeite-group
296 minerals thus form a supergroup of polysomatic series with *N* (*N'*) and *S* modules. The two

297 new species of zinconigerite from the Xianghualing skarn are the first species in the supergroup
298 shown to contain *S* modules with the approximate composition of gahnite. As such, the
299 discovery of these phases extends the range of known chemical compositions in the *N*-*S*
300 polysomatic series.

301 In terms of crystal structures, nigerite-högbomite-taaffeite supergroup minerals show
302 trigonal or hexagonal symmetry, with similar values of *a* (approximately 5.72 Å), both *N* (*N'*)
303 and *S* modules are 4.6 Å thick, and the values of *c* are multiples of 4.6 Å ($c = n \times 4.6$ Å), where
304 *n* is the total number of *N* (*N'*) and *S* modules (McKie 1963; Armbruster 2002). For subgroup-
305 2*N*1*S*, n = 3, so $c = 3 \times 4.6$ Å = 13.8 Å, and 55.2 ($12 \times 4.6$) Å for subgroup-6*N*6*S*. The phases
306 of zn-2*N*1*S* and zn-6*N*6*S* from the Xianghualing skarn have the *c* values of 13.84 Å and 55.54
307 Å, respectively. Due to the larger ionic radius of Zn than $Fe^{3+}$ and Mg, zn-2*N*1*S* has a slightly
308 larger *c* parameter than those of ferronigerite-2*N*1*S* (13.69 Å, Jacobson and Webb 1947) and
309 magnesionigerite-2*N*1*S* (13.78 Å, Chen et al. 1989), and zn-6*N*6*S* has a slightly larger *c*
310 parameter than that of magnesionigerite-6*N*6*S* (*e.g.*, 55.45 Å, Yang et al. 2013); while
311 ferronigerite-6*N*6*S* also contains about 8 wt.% ZnO, zn-6*N*6*S* has a smaller larger *c* parameter
312 (55.54 Å) than that of ferronigerite-6*N*6*S* (55.60 Å, Grey and Gatehouse 1979).

313 Chemically, zn-2*N*1*S* and zn-6*N*6*S* are similar to the 2*N*1*S*- and 6*N*6*S*-subgroups of
314 ferronigerite, respectively, but the latter having higher $Fe_2O_3$ but lower ZnO contents than the
315 former. The chemical composition of zn-6*N*6*S* is also close to zn-2*N*1*S*, but it has low contents
316 of $SnO_2$ (20.54 wt.% vs. 28.15 wt.% on average). It is easy to distinguish these two phases from
317 other minerals of nigerite group by the contents of $SnO_2$ and ZnO.

318

This is the peer-reviewed, final accepted version for American Mineralogist, published by the Mineralogical Society of America.
The published version is subject to change. Cite as Authors (Year) Title. American Mineralogist, in press.
DOI: https://doi.org/10.2138/am-2022-7983. http://www.minsocam.org/

## IMPLICATIONS

We describe two new minerals, zn-2*N*1*S* and zn-6*N*6*S*, from the Xianghualing skarn (Hunan Province, China), and provide new insights into the crystal chemistry of the *N*-*S* polysomatic series. Zn-2*N*1*S* and zn-6*N*6*S* are two new minerals of the *N*-*S* polysomatic series and are the first minerals of the series to contain the gahnite module. It may be speculated that zinconigerite subgroups with gahnite and different ratios of *N*-*S* modules, such as 2*N*2*S*, 2*N*3*S*, 2*N*4*S*, 6*N*9*S*, 6*N*12*S*, and so on, will be found in nature.

Here, both zn-2*N*1*S* and zn-6*N*6*S* are of hydrothermal origin, crystallizing during the late stages of hydrothermal metasomatism in the Xianghualing skarn; the intimate intergrowths with fluorite (Fig. 2) reflect a crystallization under F-rich conditions. The polysomatic minerals with *N* (*N'*) and *S* modules, such as ferronigerite-2*N*1*S*, ferronigerite-6*N*6*S*, magnesionigerite-6*N*6*S,* and taaffeite group minerals (Yang et al. 2013), also occur in close association with fluorite in the Xianghualing skarn. These features may suggest that high fluorine activity could promote the formation of minerals with *N* (*N'*) and *S* modules in hydrothermal fluids. However, neither of these two new phases contain F in abundances detectable by EMPA (Table 1), indicating the possible structural incompatibility of F relative to OH. Additionally, F-rich minerals in the polysomatic series of nigerite-högbomite with *N* (*N'*) and *S* modules are not found in nature. The high Fe concentration of zn-2*N*1*S* and zn-6*N*6*S* (Table 1) may suggest the continuous Fe-Zn solid-solutions of ferronigerite-2*N*1*S* – zn-2*N*1*S* and ferronigerite-6*N*6*S* – zn-6*N*6*S*. Moreover, some spinel group crystals from the Xianghualing skarn have up to 13.05 wt.% $SnO_2$ and 12.78 wt.% ZnO (Yu et al. 2018). The minerals of nigerite-högbomite polysomatic series likely originate from spinel through the exchange of (Fe + Zn) with Sn or Ti (Zakrzewski

1977). In addition, zn-2*N*1*S* and zn-6*N*6*S,* with same *N* and *S* modules but different numbers or ratio of *N* and *S* modules, are closely associated with each other in the Xianghualing skarn, likely indicating that the ordering of *N* and *S* modules during crystal growth leads to the formation of either zn-2*N*1*S* or zn-6*N*6*S*.

## ACKNOWLEDGEMENTS

We thank Sergey Aksenov, one anonymous reviewer and the technical editor for their comments and suggestions that have helped improve the quality of this paper significantly. Financial support for the research was provided by NSF of China (Grant No. 41772031).

## REFERENCES CITED

Arakcheeva, A.V., Pushcharovskii, D.Yu., Rastsvetaeva, R.K., Kashaev, A.A. and Nadezhina, T.N. (1995) Crystal structure of nigerite-6*H*. Crystallography Reports, 40, 587–592.

Armbruster, T. (2002) Revised nomenclature of högbomite, nigerite, and taafeite minerals. European Journal of Mineralogy, 14, 389–395.

Armbruster, T., Bermanec, V., Zebec, V. and Oberhänsli, R. (1998) Titanium and iron poor zincohögbomite-16*H*, $Zn_{14}(Al,Fe^{3+},Ti,Mg)_8Al_{24}O_{62}(OH)_2$, from Nezilovo, Macedonia: occurrence and crystal structure of a new polysome. Schweizerische Mineralogische und Petrographische Mitteilungen, 78, 469–477.

Armbruster, T. and Feenstra, A. (2004) Lithium in nigerite group minerals. European Journal of Mineralogy, 16:247–254.

Bannister, F. A., Hey, M. H. and Stadler, H. P. (1947) Nigerite, a new tin mineral. Mineralogical Magazine, 28, 129–136.

Brown, I.D. and Altermatt, D. (1985) Bond-valence parameters obtained from a systematic analysis of the inorganic crystal-structure database. Acta Crystallographica, B41, 244–247.

Burke, E.A.J., Lof, P. and Hazebroek, H.P. (1977) Nigerite from the Rosendal pegmatite and aplite, Kemiö island, southwestern Finland. Bulletin of the Geological Society of Finland, 49, 151–157.

Chao, C.L. (1964) Liberite $Li_2BeSiO_4$, a new lithium-beryllium silicate mineral from the Nanling Ranges, South China. Acta Mineralogica Sinica, 44(3), 334–342 (in Chinese with English abstract). - American Mineralogist, (1965), 50, 519 (abstract).

Chen, J.Z., Shi, Y.C., Pan, Z.L. and Peng, Z.Z. (1989) The crystal structure and crystal chemistry of a new mineral, penzhizongite-6H. Earth Science Journal of the Wuhan College of Geology, 14, 413–422.

Grey, I.E. and Gatehouse, B.M. (1979) The crystal structure of nigerite-24R. American Mineralogist, 64, 1255–1264.

Hejny, C. and Armbruster, T. (2002) Polysomatism in högbomite: The crystal structures of 10*T*, 12*H*, 14*T*, and 24*R* polysomes. American Mineralogist, 87, 277–292.

Higashi, T. (2001) ABSCOR. Rigaku Corporation, Tokyo.

Huang, Y. H., Du, S.H., Wang, K.H., Zhao, C.L. and Yu, Z.Z. (1958) Hsianghualite, a new beryllium mineral. Ti-chih-yueh-k'an 7, 35 (in Chinese). American Mineralogist (1960), 44, 1327–1328 (abstract).

Huang, Y.H., Du, S. H. and Zhou, X.Z. (1988) Hsianghualing rocks, deposits and minerals. Beijing Scientific Technique Press. 115–116 (in Chinese).

Jacobson, R. and Webb, J.S. (1947) The occurrence of nigerite, a new tin mineral in quartz-sillimanite-rocks from Nigeria. Mineralogical Magazine, 28, 118–128.

Mandarino, J.A. (1981) The Gladstone-Dale relationship. IV. The compatibility concept and its application. Canadian Mineralogist, 19, 441–450.

McKie, D. (1963) The högbomite polytypes. Mineralogical Magazine, 33, 563–580.

Momma, K., and Izumi, F. (2011) VESTA 3 for three dimensional visualization of crystal, volumetric and morphology data. Journal of Applied Crystallography, 44, 1272–1276.

Ockenga, E., Yal¸cin, Ü., Medenbach, O. and Schreyer, W. (1998) Zincohögbomite, a new mineral from eastern Aegean metabauxites. European Journal of Mineralogy, 10, 1361–1366.

Peacor, D. R. (1967) New data on nigerite. American Mineralogist, 52, 864–866.

Rao, C., Gu, X.P., Wang, R.C., Xia, Q.K., Cai, Y.F., Dong, C.W., Hatert, F. and Hao, Y.T. (2020) Chukochenite, IMA 2018-132a, in: CNMNC Newsletter 54; February and March 2020, page 278; European Journal of Mineralogy, 32, 275–283.

Rao, C., Hatert F., Dal Bo, F., Wang, R.C., Gu, X.P. and Baijot, M. (2017) Mengxianminite ($Ca_2Sn_2Mg_3Al_8[(BO_3)(BeO_4)O_6]_2$) a new borate mineral from Xianghualing skarn, Hunan Province, China, with a highly unusual chemical combination (B + Be + Sn). American Mineralogist, 102, 2136–2141.

Rao, C., Wang, R.C., Gu, X.P., Xia, Q.K., Dong, C.W., Hatert, F., Yu, X.G. and Wang, W.M.Y. (2018) Zinconigerite-2*N*1*S*, IMA 2018-037. CNMNC Newsletter No. 44, August 2018, page 881; European Journal of Mineralogy, 30, 877–882.

Rao, C., Gu, X.P., Wang, R.C., Xia, Q.K., Hatert, F., and Dal Bo F. (2020) Zinconigerite-6*N*6*S*, IMA 2018-122a, in: CNMNC Newsletter 56; June and July 2020, page 443; *Eur. J. Mineral*., 32,443–448.

Schmetzer, K. and Berger, A. (1990) Lamellar iron-free högbomite-24*R* from Tanzania. Neues Jahrbuch für Mineralogie Monatshefte, 1990, 401–412.

Shannon, R.D. (1976) Revised Crystal Ionic Radii and Systematic Study of Interatomic Distances in Halides and Chalcogenides. Acta Crystallographica, A32, 751–767.

Verma, A.R. and Krishna, P. (1966) Polymorphism and Polytypism in Crystals, p.154–162. Wiley, New York.

Wilson, A.J.C. (1992) International Tables for X-ray Crystallography, *Vol. C*. Kluwer Academic Press, London.

Yang, Z.M., Ding, K.S., Fourestier, J.D., Mao, Q. and Li, H. (2012) Ferrotaaffeite-2*N*'2*S*, a new mineral species, and crystal structure of $Fe^{2+}$-rich magnesiotaaffeite-2*N*'2*S* from the Xianghualing tin-polymetallic ore field, Hunan Province, China. Canadian Mineralogist, 50, 21–29.

Yang, Z.M, Ding, K.S, Fourestier, J.D, Mao, Q. and Li, H. (2013) Fe-rich Li-bearing magnesionigerite-6N6S from Xianghualing tin-polymetallic orefield, Hunan Province, P.R. China. Mineralogy and Petrology, 107, 163–169.

Yu, X.G., Rao, C., Wang, W.M.Y., Lin, X.Q. and L.X. (2018) Mineralogical behavior and metallogenic process of Sn in the Xianghualing Skarn, Hunan Province. Geological Journal of China Universities. 24(5), 645–657.

Zakrzewski, M.A. (1977) Högbomite from the Fe-Ti deposit of Linganga (Tanzania). Neues Jahrb Mineral Monatsh, 8, 373–380.

Zhong, J.L. (2014) Major types and prospecting direction of nonferrous and rare polymetallic ore deposit in Xianghualing area, South China. Geology and mineral resource of south China, 30(2), 99–108.

Zhu, J.C., Wang, R.C., Lu, J.J., Zhang, H., Zhang, W.L., Xie, L. and Zhang, R.Q. (2011) Fractionation, evolution, petrogenesis and mineralization of Laiziling granite pluton, Southern Hunan Province. Geological Journal of China Universities, 17(3), 381–392.

# Table captions:

**TABLE 1.** Chemical data of zinconigerite-2*N*1*S* and zinconigerite-6*N*6*S* from the Xianghualing skarn

**TABLE 2a.** Assigned site-occupancies in the crystal structure of zinconigerite-2*N*1*S*

**TABLE 2b.** Assigned site-occupancies in the crystal structure of zinconigerite-6*N*6*S*

**TABLE 3a.** Selected bond distances (Å) in zinconigerite-2*N*1*S*

**TABLE 3b.** Selected bond distances (Å) in zinconigerite-6*N*6*S*

**TABLE 4a.** Bond valence sums for zinconigerite-2*N*1*S*

**TABLE 4b.** Bond valence sums for zinconigerite-6*N*6*S*

# Figure captions:

**FIGURE 1.** Schematic representation of the structure ([001] projection) of nigerite-högbomite group minerals in terms of nolanite(*N*)-spinel(*S*) modules.

**FIGURE 2.** Backscattered electron (BSE) images showing occurrence and mineral associations of zinconigerite-2*N*1*S* and -6*N*6*S* from the Xianghualing skarn. (a) Euhedral zinconigerite-2*N*1*S* crystals among fluorite crystals; (b) Zinconigerite-2*N*1*S* crystals veinlets among fluorite; (c)

and (d) euhedral zinconigerite-6*N*6*S* crystals among fluorite crystals. Abbr.: 2*N*1*S* - zinconigerite-2*N*1*S*; 6*N*6*S* - zinconigerite-6*N*6*S*; Fl - fluorite; Mgt - margarite. Chb - chrysoberyl; Plg - phlogopite.

**FIGURE 3.** Raman spectra of zinconigerite-2*N*1*S* (a) and -6*N*6*S* (b) from the Xianghualing skarn.

**FIGURE 4.** Crystal structure of zinconigerite-2*N*1*S*, drawn using the VESTA 3 program (Momma and Izumi 2011).

**FIGURE 5.** Crystal structure of zinconigerite-6*N*6*S* (a) and an enlarged view of one third of the zinconigerite-6*N*6*S* structure (b), showing the 2*N* + 2*S* connectivity with the polyhedral stacking sequence of O-$T_1$-O-$T_2$-O-$T_2$-O-$T_1$. Drawn using the VESTA 3 program (Momma and Izumi 2011).

**TABLE 1.** Chemical data of zinconigerite-2*N*1*S* and zinconigerite-6*N*6*S* from the Xianghualing skarn

| **Constituent** | **Zinconigerite-2*N*1*S*** | **Zinconigerite-6*N*6*S*** |
|---|---|---|
| **Wt.%** | **n = 20** | **n = 47** |
| $Al_2O_3$ | 54.42(0.01) | 54.12(0.62) |
| $SnO_2$ | 28.15(0.56) | 20.54(0.51) |
| ZnO | 7.71(0.22) | 10.22(0.33) |
| $Fe_2O_3^*$ | 5.83(0.38) | 8.65(0.51) |
| MnO | 1.39(0.42) | 2.95(0.49) |
| MgO | 0.17(0.04) | 0.96(0.13) |
| $TiO_2$ | 0.05(0.05) | 0.41(0.19) |
| $SiO_2$ | 0.53(0.26) | 0.07(0.06) |
| CaO | 0.34(0.07) | 0.35(0.47) |
| $K_2O$ | 0.00(0.00) | 0.00(0.01) |
| $Na_2O$ | 0.36(0.14) | 0.36(0.13) |
| $H_2O^\#$ | 1.73(0.01) | 1.45(0.01) |
| Total | 100.68(0.46) | 100.09(0.61) |
| | O = 24 | O = 32 |
| Al(*apfu)* | 11.174 | 14.675 |
| Sn | 1.952 | 1.882 |
| Zn | 0.992 | 1.736 |
| Fe | 0.771 | 1.495 |
| Mn | 0.206 | 0.576 |
| Mg | 0.044 | 0.328 |
| Ti | 0.007 | 0.071 |
| Si | 0.092 | 0.017 |
| Ca | 0.063 | 0.086 |
| K | 0.000 | 0.001 |
| Na | 0.123 | 0.160 |
| H | 2.000 | 2.000 |

$^*$: calculated as $Fe^{3+}$; $H_2O^\#$: calculated on the basis of 2 (OH) *apfu*; n: number of analyses; values in parentheses: standard deviation.

This is the peer-reviewed, final accepted version for American Mineralogist, published by the Mineralogical Society of America.
The published version is subject to change. Cite as Authors (Year) Title. American Mineralogist, in press.
DOI: https://doi.org/10.2138/am-2022-7983. http://www.minsocam.org/

**TABLE 2a.** Assigned site-occupancies in the crystal structure of zinconigerite-2*N*1*S*

| Site | RSS | Site-population (*apfu*) | CSS | ABL | CBL | VS | BVS |
|---|---|---|---|---|---|---|---|
| **Sn$^{VI}$** | 46.5 | $Sn_{0.90}Al_{0.10}$ | 46.3 | 2.057 | 2.075 | 3.90 | 3.75 |
| **Zn$^{IV}$** | 21.8 | $Zn_{0.49}Al_{0.34}Mn_{0.10}Sn_{0.07}$ | 21.6 | 1.940 | 1.911 | 2.48 | 2.15 |
| **Al1$^{IV}$** | 17.5 | $Al_{0.62}Fe^{3+}_{0.38}$ | 17.9 | 1.841 | 1.808 | 3.00 | 2.68 |
| **Al2$^{VI}$** | 13.0 | $Al_{1.00}$ | 13.0 | 1.889 | 1.935 | 3.00 | 3.15 |
| **Al3$^{VI}$** | 13.0 | $Al_{1.00}$ | 13.0 | 1.918 | 1.935 | 3.00 | 2.93 |
| **Al4$^{VI}$** | 9.4 | $Al_{0.72}$ | 9.4 | 1.956 | 1.785 | 3.00 | 2.64 |

**TABLE 2b.** Assigned site-occupancies in the crystal structure of zinconigerite-6*N*6*S*

| Site | RSS | Site-population (*apfu*) | CSS | ABL | CBL | VS | BVS |
|---|---|---|---|---|---|---|---|
| **Sn$^{VI}$** | 48.5 | $Sn_{0.92}Ti_{0.08}$ | 47.8 | 2.057 | 2.083 | 4.00 | 3.93 |
| **Zn1$^{IV}$** | 21.8 | $Zn_{0.50}Fe^{3+}_{0.23}Mn_{0.14}Mg_{0.08}Al_{0.05}$ | 26.1 | 1.957 | 1.950 | 2.28 | 2.14 |
| **Zn2$^{IV}$** | 21.8 | $Zn_{0.37}Al_{0.21}Fe^{3+}_{0.20}Mn_{0.14}Mg_{0.08}$ | 23.5 | 1.924 | 1.920 | 2.41 | 2.27 |
| **Al1$^{IV}$** | 17.5 | $Al_{0.67}Fe^{3+}_{0.33}$ | 17.3 | 1.844 | 1.803 | 3.00 | 2.61 |
| **Al2$^{VI}$** | 13.0 | $Al_{1.00}$ | 13.0 | 1.915 | 1.935 | 3.00 | 2.94 |
| **Al3$^{VI}$** | 14.2 | $Al_{1.00}$ | 13.0 | 1.910 | 1.935 | 3.00 | 2.98 |
| **Al4$^{VI}$** | 13.0 | $Al_{1.00}$ | 13.0 | 1.921 | 1.935 | 3.00 | 2.91 |
| **Al5$^{VI}$** | 9.3 | $Al_{0.72}$ | 9.4 | 1.959 | 1.785 | 3.00 | 2.62 |

RSS: Refined site scattering factor ($e^-$); CSS: Calculated site scattering factor ($e^-$); ABL: average observed bond-lengths (Å); CBL: calculated bond-lengths (Å); VS: theoretical bond-valence sums (*vu*); BVS: calculated bond-valence sums (*vu*). Ideal bond-distances are calculated using the ionic radii of Shannon (1976), and the bond-valence parameters are taken from Brown and Altermatt (1985).

This is the peer-reviewed, final accepted version for American Mineralogist, published by the Mineralogical Society of America.
The published version is subject to change. Cite as Authors (Year) Title. American Mineralogist, in press.
DOI: https://doi.org/10.2138/am-2022-7983. http://www.minsocam.org/

**TABLE 3a.** Selected bond distances (Å) in zinconigerite-2*N*1*S*

| | | | | | |
|---|---|---|---|---|---|
| Sn-O4(×3) | 1.998(2) | Zn-O1 | 1.973(5) | Al1-O3 | 1.853(5) |
| Sn-O5(×3) | 2.114(3) | Zn-O2(×3) | 1.924(2) | Al1-O5(×3) | 1.832(2) |
| <Sn-O> | 2.056 | <Zn-O> | 1.936 | <Al-O> | 1.837 |
| Al3-O1 | 1.924(3) | Al4-O5(×4) | 1.977(3) | Al2-O2(×6) | 1.899(3) |
| Al3-O2(×2) | 1.949(2) | Al4-O6(×2) | 1.914(2) | <Al-O> | 1.899 |
| Al3-O3 | 1.951(3) | <Al-O> | 1.956 | | |
| Al3-O4(×2) | 1.873(2) | | | | |
| <Al-O> | 1.920 | | | | |

**TABLE 3b.** Selected bond distances (Å) in zinconigerite-6*N*6*S*

| | | | | | |
|---|---|---|---|---|---|
| Sn-O3(×3) | 2.106(3) | Zn1-O4 | 1.952(4) | Zn2-O2 | 1.960(4) |
| Sn-O6(×3) | 2.002(1) | Zn1-O5(×3) | 1.960(1) | Zn2-O7(×3) | 1.921(2) |
| <Sn-O> | 2.054 | <Zn-O> | 1.958 | <Zn-O> | 1.931 |
| Al1-O3(×3) | 1.834(2) | Al2-O2(×2) | 1.943(1) | Al3-O5(×3) | 1.919(2) |
| Al1-O8 | 1.864(4) | Al2-O5(×4) | 1.902(1) | Al3-O7(×3) | 1.896(2) |
| <Al-O> | 1.842 | <Al-O> | 1.916 | <Al-O> | 1.908 |
| Al4-O4 | 1.905(2) | Al5-O1(×2) | 1.911(2) | | |
| Al4-O6(×2) | 1.873(1) | Al5-O3(×4) | 1.981(3) | | |
| Al4-O7(×2) | 1.961(2) | <Al-O> | 1.958 | | |
| Al4-O8 | 1.948(2) | | | | |
| <Al-O> | 1.920 | | | | |

This is the peer-reviewed, final accepted version for American Mineralogist, published by the Mineralogical Society of America.
The published version is subject to change. Cite as Authors (Year) Title. American Mineralogist, in press.
DOI: https://doi.org/10.2138/am-2022-7983. http://www.minsocam.org/

**TABLE 4a.** Bond valence sums for zinconigerite-2*N*1*S*

| | Sn | Zn | Al1 | Al2 | Al3 | Al4 | Σ |
|---|---|---|---|---|---|---|---|
| **O1** | | 0.489 | | | 0.478(×3→) | | **1.92** |
| **O2** | | 0.559(×3↓) | | 0.525(×6↓) | 0.447(×2→)(×2↓) | | **1.98** |
| **O3** | | | 0.647(×3↓) | | 0.444(×3→) | | **1.98** |
| **O4** | 0.726(×3↓) | | | | 0.5490(×2→)(×2↓) | | **1.82** |
| **O5** | 0.531(×3↓) | | 0.685(×3↓) | | | 0.415(×2→)(×4↓) | **2.05** |
| **O6** | | | | | | 0.491(×3→)(×2↓) | **1.47** |
| **Σ** | **3.77** | **2.17** | **2.70** | **3.15** | **2.91** | **2.64** | |

**TABLE 4b.** Bond valence sums for zinconigerite-6*N*6*S*

| | Sn1 | Zn1 | Zn2 | Al1 | Al2 | Al3 | Al4 | Al5 | Σ |
|---|---|---|---|---|---|---|---|---|---|
| **O1** | | | | | | | | 0.495(×3→)(×2↓) | **1.49** |
| **O2** | | | 0.516 | | 0.454(×3→)(×2↓) | | | | **1.88** |
| **O3** | 0.570(×3↓) | | | 0.671(×2→)(×3↓) | | | | 0.410(×4↓) | **2.06** |
| **O4** | | 0.542 | | | | | 0.503(×3→) | | **2.05** |
| **O5** | | 0.530(×3↓) | | | 0.507(×4↓) | 0.485(×2→)(×3↓) | | | **2.03** |
| **O6** | 0.755(×2→)(×3↓) | | | | | | 0.549(×2↓) | | **1.85** |
| **O7** | | | 0.573(×3↓) | | | 0.516(×3↓) | 0.433(×2→)(×2↓) | | **1.95** |
| **O8** | | | | 0.619(×3↓) | | | 0.448(×3→) | | **1.96** |
| **Σ** | **3.97** | **2.13** | **2.24** | **2.63** | **2.94** | **3.00** | **2.91** | **2.63** | |

This is the peer-reviewed, final accepted version for American Mineralogist, published by the Mineralogical Society of America.
The published version is subject to change. Cite as Authors (Year) Title. American Mineralogist, in press.
DOI: https://doi.org/10.2138/am-2022-7983. http://www.minsocam.org/

Figure 1

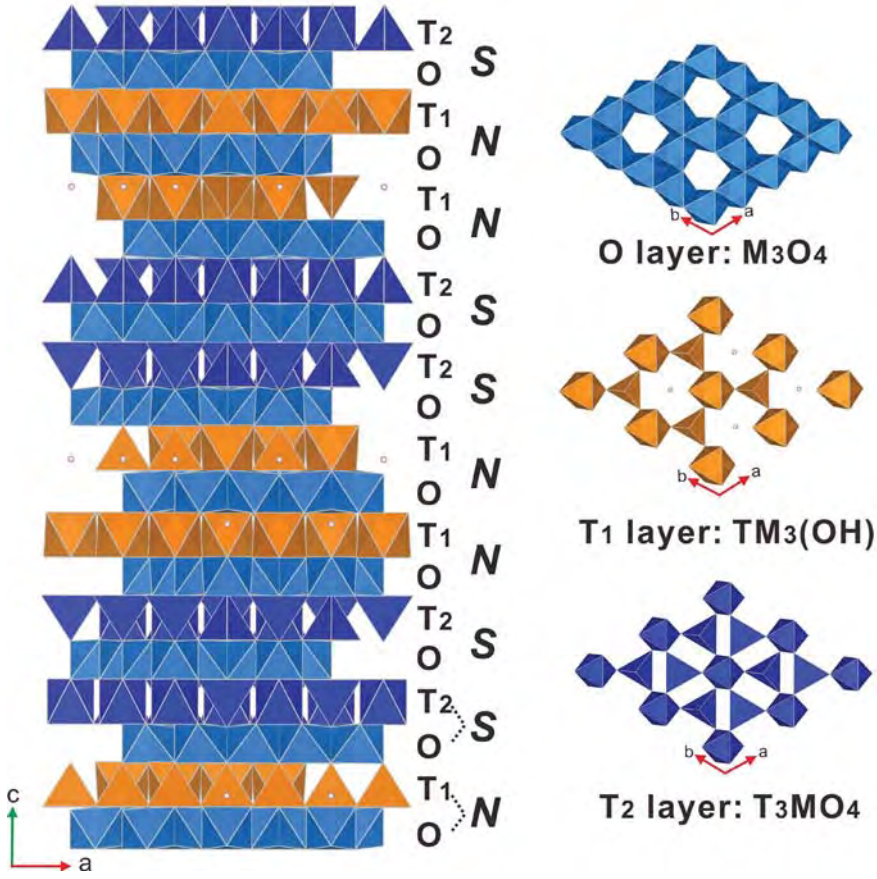

Figure 2

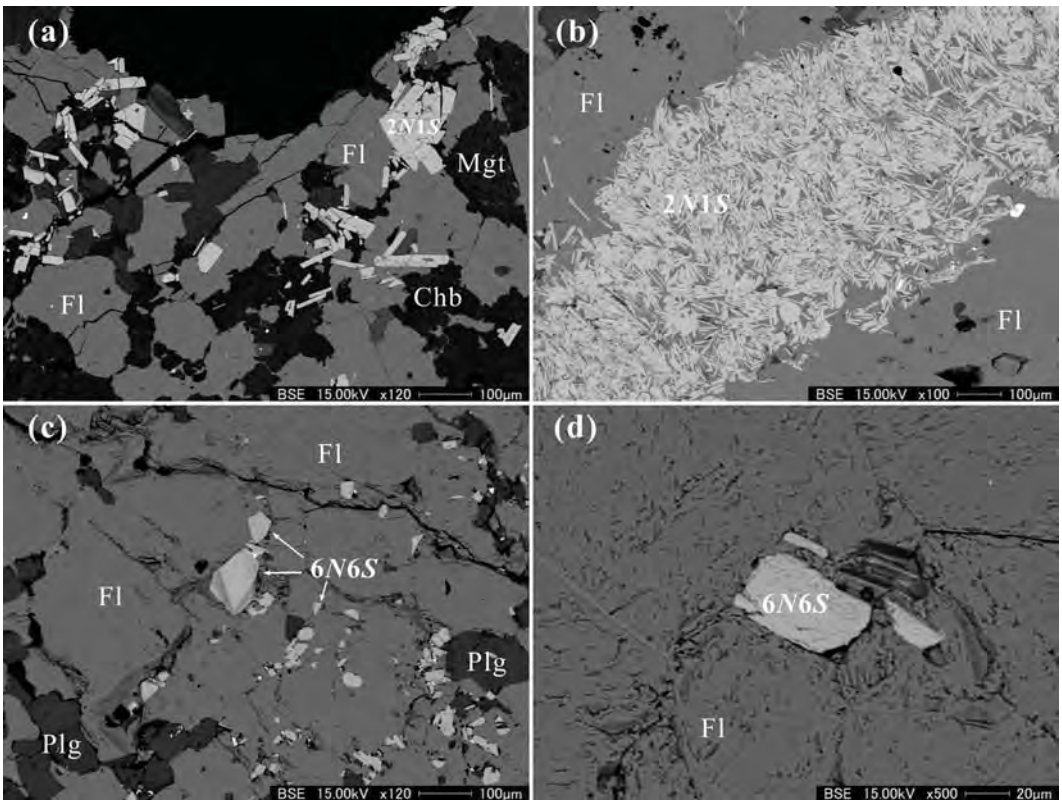

This is the peer-reviewed, final accepted version for American Mineralogist, published by the Mineralogical Society of America.
The published version is subject to change. Cite as Authors (Year) Title. American Mineralogist, in press.
DOI: https://doi.org/10.2138/am-2022-7983. http://www.minsocam.org/

Figure 3

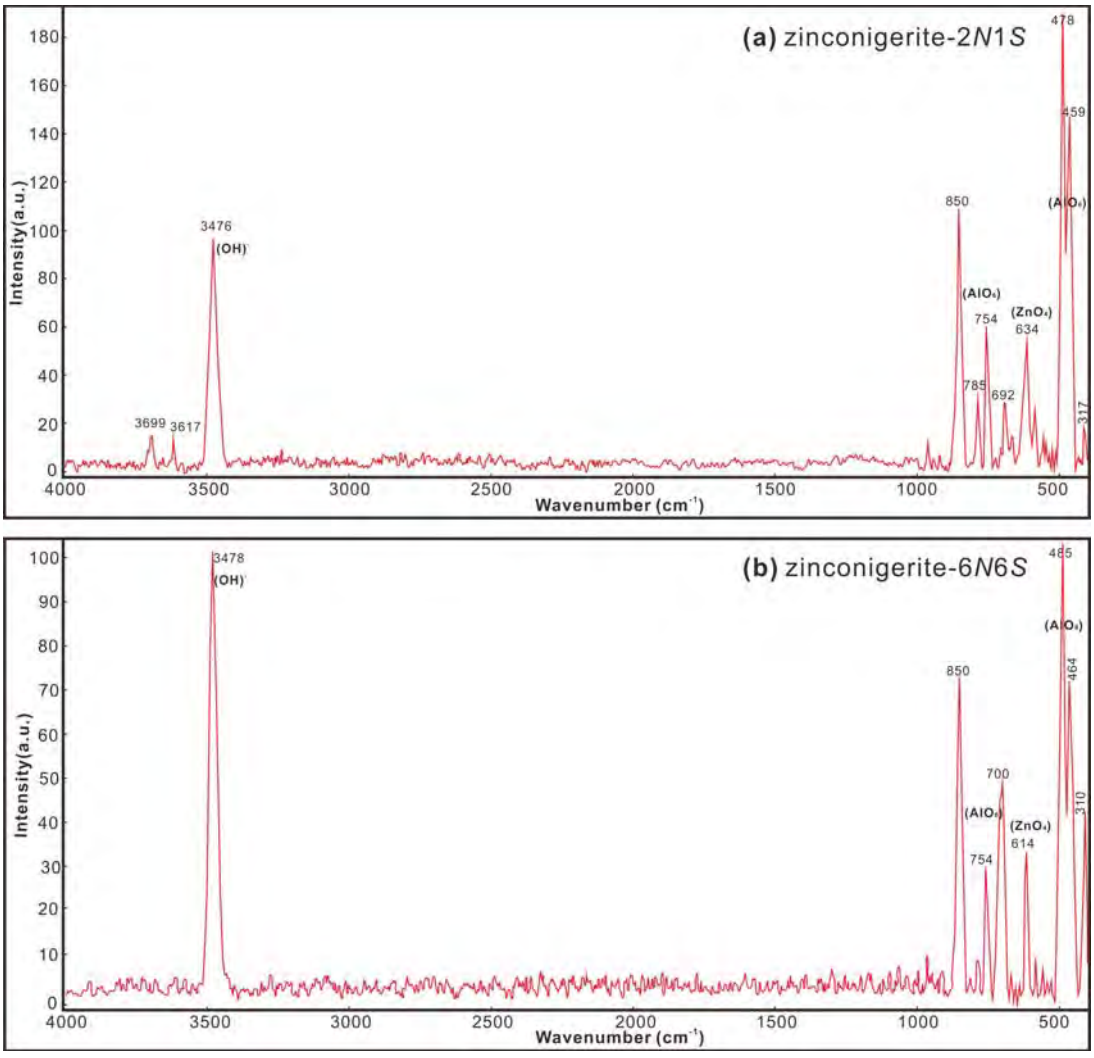

Figure 4

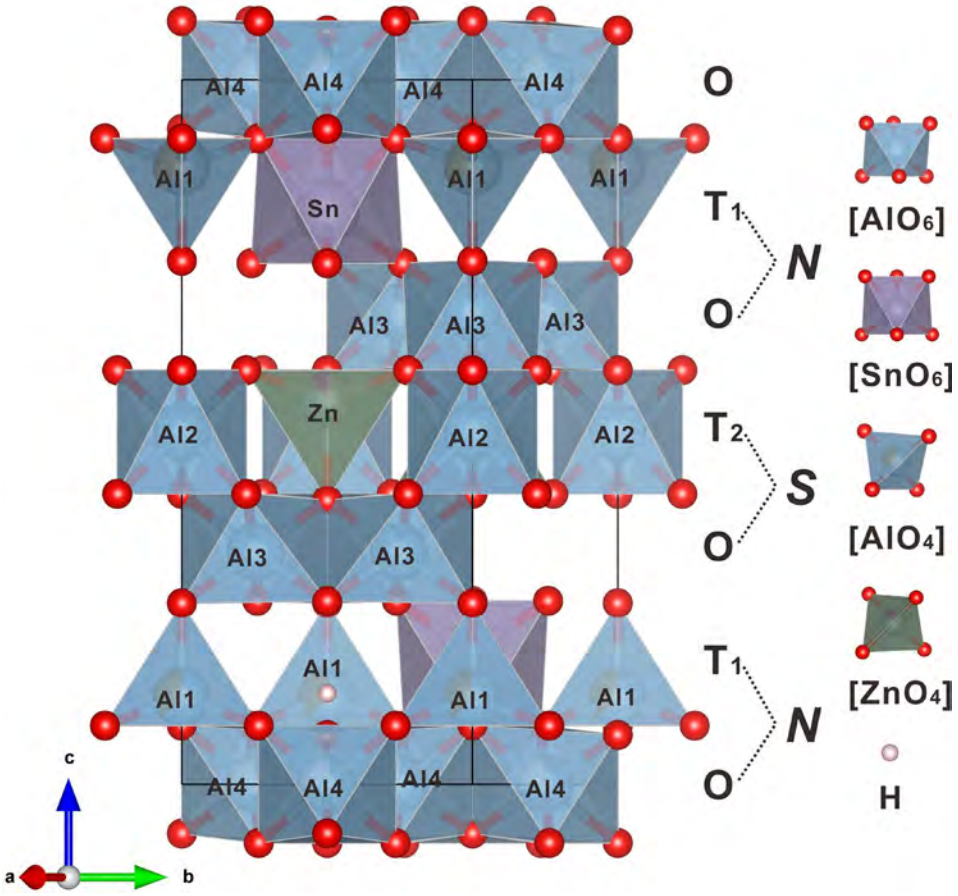

This is the peer-reviewed, final accepted version for American Mineralogist, published by the Mineralogical Society of America.
The published version is subject to change. Cite as Authors (Year) Title. American Mineralogist, in press.
DOI: https://doi.org/10.2138/am-2022-7983. http://www.minsocam.org/

Figure 5